Molecular-Brownian Correspondence in the Hard-sphere Dynamic Universality Class

Leticia López-Flores[1], Martín Chávez-Páez[2], Magdaleno Medina-Noyola[2]
[1] *Facultad de Ciencias Fisico-Matemáticas, Benemérita Universidad Autónoma de Puebla, Apartado Postal 1152, 72000 Puebla, Pue., México and*
[2] *Instituto de Física "Manuel Sandoval Vallarta", Universidad Autónoma de San Luis Potosí, Álvaro Obregón 64, 78000 San Luis Potosí, SLP, México*

(Dated: February 15, 2013)

We perform systematic simulation experiments on model systems with soft-sphere repulsive interactions to test the predicted dynamic equivalence between soft-sphere liquids with similar static structure. For this we compare the simulated dynamics (mean squared displacement, intermediate scattering function, α-relaxation time, etc.) of different soft-sphere systems, between them and with the hard-sphere liquid. We then show that the referred dynamic equivalence does not depend on the (Newtonian or Brownian) nature of the microscopic laws of motion of the constituent particles, and hence, applies independently to colloidal and to atomic simple liquids. In addition, we verify another more recently-proposed dynamic equivalence, this time between the *long-time* dynamics of a Brownian fluid and its corresponding atomic liquid (i.e., the atomic system with the same interaction potential).

PACS numbers: 23.23.+x, 56.65.Dy

INTRODUCTION

At first sight, the macroscopic dynamics of supercooled liquids seems to be strongly material-specific, with no universal character at all. This is evidenced, for example, by the great diversity of molecular glass formers (ionic, metallic, organic, polymeric, etc.), giving rise to an overwhelmingly rich phenomenology [1–5]. One can easily understand this lack of universal behavior in terms of the wide differences in the materials' structure and composition, the masses of their individual atoms, their preparation protocol, etc. Of course, the scenario becomes even more complex when one attempts to include colloidal systems in the discussion.

The formation of colloidal glasses and gels has been the subject of intense study during the last two decades [6], and it is a widespread notion that the phenomenology of both, the glass transition in "thermally-driven" molecular glass formers, and the dynamic arrest transition in "density-driven" hard-sphere colloidal systems, might share a common underlying universal origin [7]. Two relevant conceptual issues, however, must be understood in order for this expectation to have a more fundamental basis. The first one requires us to spell out the manner in which undercooling an atomic liquid might be equivalent to overcompressing a colloidal liquid. The second is to clarify under what conditions the macroscopic dynamics of both classes of systems could be expected to be equivalent, given the fact that the microscopic dynamics is Newtonian in atomic liquids and Brownian in colloidal fluids.

The answer to these two questions is highly relevant since it will allow us to understand which aspects of the macroscopic dynamics of a given system are universal and which ones are system-specific. These two issues have been addressed using computer simulation methods on well defined model systems. For example, interesting scalings of the *equilibrium* dynamics of simple models of soft-sphere glass formers have been exposed by systematic computer simulations [8, 9], which provide an initial clue to the possible physical origin of the equivalence between the process of cooling and the process of compression. Similarly, also using computer simulations, it has been partially corroborated that standard molecular dynamics will lead to essentially the same dynamic arrest scenario as Brownian dynamics for a given model system (i.e., same pair potential) [10–12].

From the theoretical side it would be desirable to have a unified description of the macroscopic dynamics of both, colloidal and atomic liquids, which explicitly predicts the aspects of the macroscopic dynamics that are expected to be universal. These topics might be addressed in the framework of a theory such as the mode coupling theory of the ideal glass transition [13]. In fact, the similarity of the long-time dynamics of Newtonian and Brownian systems in the neighborhood of the glass transition, for example, has been studied within this theoretical framework [14]. A number of issues, however, still remain open [11].

The present paper is part of an effort aimed at addressing these two fundamental issues within a general theoretical framework, namely, the generalized Langevin equation (GLE) formalism [15–17]. This formalism was employed in the construction of the self-consistent generalized Langevin equation (SCGLE) theory of colloid dynamics [18–20], eventually applied to the description of dynamic arrest phenomena [21–23], and more recently, to the construction of a first-principles theory of equilibration and aging of colloidal glass-forming liquids [24, 25].

When applied to model systems with soft repulsive interactions [26], the SCGLE theory of colloid dynamics, together with the condition of static structural equiv-

alence between soft- and hard-sphere systems, predicts the existence of a "hard-sphere dynamic universality class", constituted by the soft-sphere systems whose dynamic parameters, such as the α-relaxation time and self-diffusion coefficient, depend on density, temperature and softness in a universal scaling fashion [27], through an effective hard-sphere diameter determined by the Andersen-Weeks-Chandler [28, 29] criterion. These predictions provide a more fundamental explanation of the scalings previously exhibited by computer simulations [8, 9], and point to the physical basis of the dynamic equivalence between cooling and compressing.

The main purpose of this paper is to report the results of, and to provide detailed technical information on, a number of simulation experiments performed with the purpose of testing this density-temperature-softness scaling in the referred dynamic universality class. An illustrative selection of these results were advanced in a recent brief communication [27]. The second main purpose of the present paper is to perform the pertinent simulation experiments to test a second relevant prediction of the SCGLE theory, which addresses the second of the two fundamental issues mentioned above, namely, the macroscopic dynamic equivalence between atomic and colloidal liquids. As it happens, the SCGLE theory of colloid dynamics is being extended to describe the dynamics of simple atomic liquids [30, 31]. The scenario that emerges from these theoretical developments include well defined scaling rules that exhibit the equivalence between the dynamics of colloidal fluids and the *long-time* dynamics of atomic liquids. Here we test these scalings by comparing the simulation results for a given model system using both, molecular dynamics and Brownian dynamics simulations.

Thus, the present paper is essentially a report of a set of systematic computer simulations, and in Sec. we define the interaction potentials of the model systems considered in our study and provide the basic information on the simulation methods employed. In Sec. we review the concept of static structural equivalence between soft- and hard-sphere fluids, and explain how this concept is employed to map the static structure of any soft-sphere liquid onto the properties of an effective hard-sphere liquid. In Sec. we review the extension of this structural equivalence to the dynamic domain and present the simulation results that validate the accuracy of the resulting dynamic equivalence between soft- and hard-sphere liquids. Here we first verify that this dynamic equivalence is exhibited by the results of our Brownian dynamics simulations, and then confirm that the same dynamic equivalence is also observed in the results of our molecular dynamics simulations. In Sec. we explain the correspondence between the dynamics of colloidal fluids and the *long-time* dynamics of atomic liquids, and verify that the predicted scalings are indeed satisfied by our molecular and Brownian dynamics simulations. At this point we have to mention that the present study only involves Brownian dynamics simulations that completely ignore the effects of hydrodynamic interactions, which have an enormous practical relevance in concentrated colloidal fluids. In the last section, besides summarizing the main results of this paper, we explain that for the systems with interaction potential in the hard sphere dynamic universality class, these effects can be taken into account through the value of the short-time self-diffusion coefficient, thus expanding the applicability of the scalings discussed here.

METHODOLOGICAL ASPECTS

In this section we describe the most relevant methodological aspects of this work. This includes information on the numerical simulation methods and on the theoretical concepts and approaches employed.

Model potentials

Let us consider a model liquid formed by N spherical particles in a volume V which interact through a soft repulsive pair potential $u(r)$ with tunable softness. We intend to study the interplay of the effects of the number density (or concentration, in the case of colloidal liquids) $n \equiv N/V$, temperature T, and softness, represented by some parameter denoted generically as ν. There is a variety of analytic proposals for such tunable soft potential [8, 9], but for concreteness here we shall refer explicitly to three specific representative model systems. The first is the truncated Lennard-Jones–like (TLJ) potential,

$$u^{(\nu)}(r) = \epsilon \left[\left(\frac{\sigma}{r}\right)^{2\nu} - 2\left(\frac{\sigma}{r}\right)^{\nu} + 1 \right] \Theta(\sigma - r), \quad (1)$$

in which $\Theta(x)$ is the unit step function. The positive parameter ν controls the softness of the interaction, with the limit $\nu \to \infty$ corresponding to the hard sphere potential between particles of diameter σ. For fixed ν, the state space of this system is spanned by the dimensionless temperature $T^* \equiv k_B T/\epsilon$ and volume fraction $\phi = \pi n \sigma^3/6$.

The specific form of Eq. (1) differs qualitatively from the inverse power-law (IPL) potential

$$u(r) = \epsilon(\sigma/r)^{2\nu}, \quad (2)$$

commonly used to model hard sphere effects. Just like in the case of the TLJ model, for fixed softness parameter ν the state space of the IPL model system is also spanned by the dimensionless temperature $T^* \equiv k_B T/\epsilon$ and volume fraction $\phi = \pi n \sigma^3/6$. The fundamental difference between the IPL potential and the TLJ interaction is that the latter is always short-ranged.

The third interaction model that we shall refer to is defined by the hard-sphere plus repulsive Yukawa (HSY) potential, frequently used to model the screened electrostatic repulsions between charged colloidal particles [32]. This is defined here as

$$u(r) = \epsilon \left[\frac{\exp[-z(r/\sigma - 1)]}{(r/\sigma)} \right]. \qquad (3)$$

For fixed screening parameter z, the state space of this system is also spanned by the volume fraction $\phi = \pi n \sigma^3/6$ and the dimensionless temperature $T^* \equiv k_B T/\epsilon$ (sometimes, however, we shall also refer to the repulsion intensity parameter $K \equiv 1/T^* = \beta\epsilon$). The inverse screening length z controls the range of the potential, and for our purpose, we may consider that it plays the role of the softness parameter. Typical values for these parameters representing real suspensions of highly charged colloidal suspensions at low ionic strength in the dilute regime are $K = 554$, $z = 0.149$, and ϕ of the order of 10^{-4} [33]. We shall use these as illustrative values, along with $K = 100$ and $z = 1.0$. Figure (1) plots these interaction models for some specific values of these parameters to illustrate the variety of interactions considered.

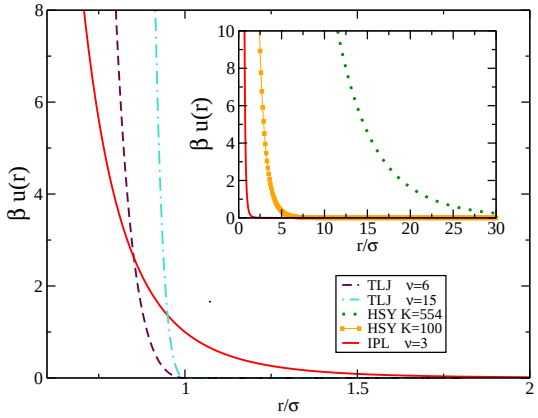

FIG. 1: Illustration of the TLJ, IPL, and HSY potentials.

Simulation aspects

Molecular dynamics (MD) simulations using the velocity-verlet algorithm [34] were conducted for the model liquids above, formed by N spherical particles of mass M in a simulation box of volume V. The results are expressed in the well known Lennard-Jones units, where M, σ and ϵ are taken as the units of mass, length, and energy, respectively, and $t_{MD} = \sqrt{M\sigma^2/\epsilon T^*}$ is the corresponding time unit.

For Brownian dynamics (BD) simulations we follow the prescription proposed by Ermak and Mcammon [34] to evolve the positions of the particles in the simulation box. Thus, for a given particle at the position $\vec{r}(t)$ and under the force $\vec{F}(t)$, the particle is displaced in the α direction according to

$$r_\alpha(t + \Delta t) = r_\alpha(t) + \beta D^0 F_\alpha(t)\Delta t + R_\alpha \qquad (4)$$

where D^0 is the short-time self-diffusion coefficient of the particle, Δt is the time step, and R_α is a random displacement extracted from a Gaussian distribution with zero mean and variance $2D^0\Delta t$. Taking σ as the length unit and ϵ as the energy unit, $t_{BD} \equiv \sigma^2/D^0$ becomes the natural time scale.

In both cases, the simulations were conducted with $N = 1000$ particles in a cubic simulation box with periodic boundary conditions. The initial configurations were generated using the following procedure. First, particles were placed randomly in the simulation box at the desired density, such that the maximum overlap between particles was in the range $0.65\sigma - 0.8\sigma$. To relax this initial configuration and reduce or eliminate the overlap between the particles we tried two methods. In one of them we perform Monte Carlo cycles [35] at a high temperature, and then decrease the temperature for several steps until the original temperature was restored. In the other method we uniformly expand the system by increasing the length of the simulation box by a factor of at least 1.5. Then, we run MD or MC cycles while decreasing the simulation box until the original value was reached. We checked that the these two methods produce equivalent results. Once the initial configuration is constructed, several thousand cycles are performed to lead the systems to equilibrium, followed by at least two million cycles where the data is collected. In the case of MD simulations, temperature was kept constant by simple rescaling of the velocities of the particles every 100 time steps [34].

Several structural and dynamic quantities are calculated from the equilibrium configurations generated in the simulations. In particular, the radial distribution function $g(r)$ was calculated using the standard approach [34]. The static structure factor $S(k)$ can then be obtained as

$$S(k) = 1 + 4\pi n \int [g(r) - 1] \frac{\sin(kr)}{kr} r^2 dr. \qquad (5)$$

Alternatively, $S(k)$ can be calculated directly from the positions of the particles in the simulation box [29].

Time correlation functions, like the mean squared displacement (MSD)

$$W(t) = \left\langle (\Delta\vec{r}(t))^2 \right\rangle /3, \qquad (6)$$

and the self-intermediate scattering function $F_S(k,t)$,

$$F_S(k,t) = \left\langle \frac{1}{N}\sum_{j=1}^{N} \exp(-i\vec{k}\cdot\vec{\Delta}r_j(t)) \right\rangle, \qquad (7)$$

where $\Delta\vec{r}_j = \vec{r}_j(t) - \vec{r}_j(0)$, were calculated using the efficient, low-memory algorithm proposed in Ref. [36].

Crystallinity of the systems was monitored through the order parameters Q_l, especially Q_6, defined as

$$Q_l = \left[\frac{4\pi}{2l+1} \sum_{m=-l}^{l} |Q_{lm}|^2 \right]^{1/2}, \qquad (8)$$

where Q_{lm} is basically the average, over all particles, of the mean spherical harmonics $Y_{lm}(\hat{r}_{ij})$ established between each particle i and its close neighbors ($j = 1, ..., N_b(i)$), where $N_b(i)$ is the number of neighbors of the particle [37]. Since in this paper we are interested only in the amorphous liquid state, when the simulations of monodisperse systems exhibited crystalline order, thus indicating that the corresponding volume fraction was beyond the freezing point, we discarded that monodisperse run, and performed an alternative simulation introducing size polydispersity to frustrate crystallization. Polydispersity is handled following a previous work [38], where the diameters of the N particles are taken to be evenly distributed between $\bar{\sigma}(1 - w/2)$ and $\bar{\sigma}(1 + w/2)$, with $\bar{\sigma}$ being the mean diameter. We consider the case $w = 0.3$, corresponding to a polydispersity $P = w/\sqrt{12} = 0.0866$. Let us emphasize that this procedure was followed in both, molecular and Brownian dynamics simulations, and that in both cases only size polydispersity was introduced, leaving all the other parameters unchanged (such as the mass or the short-time self-diffusion coefficient of the particles).

At this point, it is important to emphasize that when the system remains in its metastable liquid phase, the equilibration time increases enormously as the system approaches its dynamic arrest transition (see the detailed discussion in Ref. [38]). This means that as the volume fraction increases in the metastable region, the initial equilibration period will eventually be insufficient, and will need to be adjusted to make sure that the system indeed equilibrated properly, as recommended in [38]. The present study, however, is not aimed at studying the equilibration process by itself, and hence, we shall avoid approaching too close to the glass transition, so as to focus our attention on the subject of this work, namely, on the dynamic equivalence between soft-sphere liquids.

To illustrate the end result of this procedure, in Figure (2) we show the corresponding MSD for the TLJ system ($\nu = 15$) in the previous figure for volume fractions in an extended range, namely, $\phi = 0.1, 0.4, 0.5, 0.6, 0.7$. These results fully cover the stable fluid phase and much of the metastable liquid regime. In all samples the MSD clearly exhibits the ballistic and diffusive time regimes typical of atomic liquids. We note that the monodisperse system with $\phi = 0.65$ is highly ordered. Hence, we simulate instead a polydisperse system whose volume fraction $\phi \equiv V^{-1}\sum_{i=1}^{N} \pi\sigma_i^3/6$ is set to the value $\phi = 0.65$.

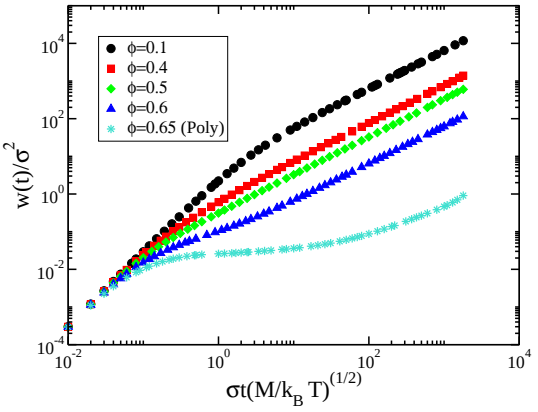

FIG. 2: Mean squared displacement from MD simulations for monodisperse TLJ systems with $\nu = 15$ and several values of the volume fraction ($\phi = 0.1, 0.4, 0.5, 0.6$). The most concentrated system is polydisperse, with volume fraction $\phi = 0.65$.

SOFT-HARD STATIC EQUIVALENCE

Although simulations are the main methodology employed here to generate the static and the dynamic information of the model systems above, the analysis of this information will rely on a few theoretical notions, most notably the predicted static and dynamic equivalence between soft-sphere and hard-sphere liquids. In this analysis, however, we shall recurrently need the *exact* structural properties of the fluid of hard-spheres of diameter σ and volume fraction ϕ, embodied in its RDF $g_{HS}(r/\sigma;\phi)$ or in its static structure factor $S_{HS}(k\sigma;\phi)$. For these structural properties a virtually exact representation is provided by the Percus-Yevick [39, 40] approximation with its Verlet-Weis correction, defined as [41]

$$g_{HS}(r/\sigma;\phi) = g^{(PY)}(r/\sigma_w;\phi_w), \qquad (9)$$

and

$$S_{HS}(k\sigma;\phi) = S^{(PY)}(k\sigma_w;\phi_w), \qquad (10)$$

with the parameters ϕ_w and σ_w defined as

$$\phi_w \equiv \phi - \phi^2/16, \qquad (11)$$

and

$$\sigma_w \equiv \sigma(\phi_w/\phi)^{1/3}. \quad (12)$$

The functions $g^{(PY)}(x;\phi)$ and $S^{(PY)}(y;\phi)$ are the solution of the Ornstein-Zernike equation with Percus-Yevick closure for the HS fluid provided, for example, by Wertheim [40] as easily programmable analytic expressions. The resulting $g_{HS}(r/\sigma;\phi)$ will be employed recurrently in the practical implementation of the concept of *static structural* equivalence between soft- and hard-sphere systems. This notion was first introduced as an essential aspect of the equilibrium perturbation theory of liquids [28, 29, 41].

Let us consider a model liquid formed by spherical particles interacting through any soft repulsive potential $u(r)$ with tunable softness, such as the TLJ potential in Eq. (1). The equilibrium static structure of this generic system is represented by the radial distribution function (RDF) $g(r;n,T;\sigma,\epsilon,\nu)$, also written in terms of dimensionless variables as $g(r/\sigma;\phi,T^*,\nu)$, with $T^* \equiv k_BT/\epsilon$ and $\phi = \pi n\sigma^3/6$. The physical notion behind the principle of static equivalence is that at any state point (ϕ,T^*,ν), this soft-sphere system is structurally identical to a hard-sphere system with a state-dependent effective hard-sphere diameter σ_{HS} and effective number density n_{HS}. This means that for any state point (ϕ,T^*,ν) one can find a diameter $\sigma_{HS} = \sigma_{HS}(\phi,T^*,\nu)$ and a number density $n_{HS} = n_{HS}(\phi,T^*,\nu)$ such that $g(r;n,T;\sigma,\epsilon,\nu) \approx g_{HS}(r;n_{HS},\sigma_{HS})$ [28, 29, 41], where $g_{HS}(r;n_{HS};\sigma_{HS})$ is the radial distribution function of the HS system, also written as $g_{HS}(r/\sigma_{HS};\phi_{HS})$, with $\phi_{HS} = \pi n_{HS}\sigma_{HS}^3/6$. This condition for structural equivalence can thus be written in terms of dimensionless variables as

$$g\left(\frac{r}{\sigma};\phi,T^*,\nu\right) \approx g_{HS}(\frac{r}{\sigma_{HS}};\phi_{HS}), \quad (13)$$

with

$$\phi_{HS} = \frac{\pi}{6}n_{HS}\sigma_{HS}^3 = \lambda_n\lambda_\sigma^3\phi, \quad (14)$$

where λ_σ is just the state-dependent effective hard-sphere diameter in units of σ,

$$\lambda_\sigma(\phi,T^*,\nu) \equiv \sigma_{HS}(\phi,T^*,\nu)/\sigma. \quad (15)$$

and λ_n is the state-dependent HS particle number density in units of n,

$$\lambda_n(\phi,T^*,\nu) \equiv n_{HS}(\phi,T^*,\nu)/n. \quad (16)$$

Thus, the condition for structural equivalence can thus be written in scaled form as

$$g\left(\frac{r}{\sigma};\phi,T^*,\nu\right) \approx g_{HS}\left(\lambda_\sigma^{-1}\frac{r}{\sigma};\lambda_n\lambda_\sigma^3\phi\right). \quad (17)$$

This equivalence condition can be used in several manners. The first one is to determine the parameters σ_{HS} and n_{HS} that correspond to a given soft-sphere system at a given state, i.e., to determine the functions $\sigma_{HS} = \sigma_{HS}(\phi,T^*,\nu)$ and $n_{HS} = n_{HS}(\phi,T^*,\nu)$. This might be done theoretically, using specific assumptions. For example, one could assume that $n_{HS} = n$ and that σ_{HS} is ϕ-independent, with $\sigma_{HS} = \sigma_{HS}(T^*,\nu)$ determined by means of an approximate version of the equivalence condition in Eq. (13). For example, the approximation employed in the so-called blip-function method reads in general [29]

$$\int_0^\infty 4\pi r^2\left[e^{-\beta u(r)} - e^{-\beta u_{HS}(r)}\right]dr = 0, \quad (18)$$

which for the TLJ system can be written as

$$\lambda_\sigma^3(T^*,\nu) = 1 - 3\int_0^1 dx x^2 \exp\left[-\frac{1}{T^*}(\frac{1}{x^{2\nu}} - \frac{2}{x^\nu} + 1)\right]. \quad (19)$$

Evaluating $\lambda_\sigma(T^*,\nu)$ determines σ_{HS} as $\sigma_{HS}(T^*,\nu) = \sigma\lambda_\sigma(T^*,\nu)$.

Naturally, this or any other approximate scheme has a limited range of validity. For example, as we shall see shortly, the blip function method is reasonably accurate for finite-range, moderately soft potentials, such as the TLJ liquid with softness parameter $\nu \gtrsim 6$, but it fails completely for systems with much softer and longer-ranged potentials, such as the HSY fluid with $K = 554$, $z = 0.149$, and ϕ of the order of 10^{-4}. Thus, it is important to search for a more robust method to determine the functions $\sigma_{HS} = \sigma_{HS}(\phi,T^*,\nu)$ and $n_{HS} = n_{HS}(\phi,T^*,\nu)$.

One possible method, proposed in Ref. [42], is to determine the volume fraction of the HS system whose radial distribution function provides the best overall fit of the exact RDF $g(r/\sigma;\phi,T^*)$ of the soft-sphere liquid previously determined, for example, by computer simulations. This method is illustrated here in Fig. (3), where we plot simulation data for the RDF of three soft-sphere model potentials (TLJ, IPL, and HSY). Fig. (3a), for example, plots the RDF $g(r/\sigma;\phi,T^*,\nu)$ of the TLJ liquid with $\nu = 6$, $T^* = 1$, and $\phi = 0.7$. Thus, we first determine the effective hard sphere volume fraction ϕ_{HS} by plotting the exact RDF $g_{HS}(r/\sigma_{HS};\phi_{HS})$ of Eq. (9) for various volume fractions until we identify the value of ϕ_{HS} such that the height of its second maximum matches the height of the second maximum of the soft sphere RDF (≈ 1.37, indicated by the thin horizontal line in the figure). The solid curve is the resulting hard sphere RDF.

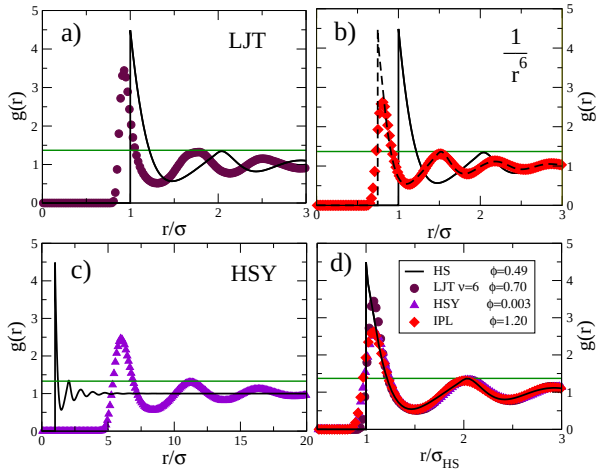

FIG. 3: Radial distribution function for (a) TLJ, (b) IPL, and (c) Yukawa systems at the equivalent volume fraction $\phi_{HS} = 0.49$. The thick line corresponds to the solution of OZ-PY-VW theory for hard spheres.

This procedure assigns a unique value of ϕ_{HS} to that set of values of the parameters (ϕ, T^*, ν), i.e., it determines the function $\phi_{HS} = \phi_{HS}(\phi, T^*, \nu)$. As observed in figure (3a), the height of these two second maxima of $g(r)$ coincide, but their positions differ. One finds, however, that a simple linear rescaling $r \to \lambda_\sigma r$ of the radial coordinate of this HS RDF, prescribed by the equivalence condition in Eq. (17), suffices to match the position of the two second maxima. This rescaling determines the parameter λ_σ, and hence, also the effective hard-sphere diameter σ_{HS} at the state point (ϕ, T^*, ν) as $\sigma_{HS} = \sigma\lambda_\sigma(\phi, T^*, \nu)$. Finally, the function $n_{HS} = n_{HS}(\phi, T^*, \nu)$ is determined by

$$n_{HS} = n\left(\frac{\phi_{HS}}{\phi}\right)\left(\frac{\sigma}{\sigma_{HS}}\right)^3. \qquad (20)$$

Following this procedure in the illustrative example in Fig. (3a) we find that $\phi_{HS} = 0.49$ and $\lambda_\sigma = \sigma_{HS}/\sigma = 0.88$; as a consequence we find that $\lambda_n = n_{HS}/n = 1.027$. These numbers differ only slightly from the results of the blip function method, which assumes $\lambda_n = 1$ and determines that $\lambda_\sigma = 0.888$ and $\phi_{HS} = 0.49$, a comparison that illustrates the accuracy of the blip function method for the TLJ potential with $\nu = 6$. This accuracy improves for more rigid potentials and deteriorates for softer and longer-ranged ones.

For example, Fig. (3b) reports an identical exercise for the IPL potential with $\nu = 3$, $T^* = 1$, and $\phi = 1.2$, whose RDF is represented by the symbols in the figure. Here again the solid line is the RDF of the equivalent HS system as a function of r/σ_{HS} and the dashed line is the same RDF, but now plotted as a function of r/σ, to illustrate the overall agreement between the RDF of the soft-sphere system and that of the equivalent HS system. This method determines the effective HS parameters $\phi_{HS} = 0.49$, $\lambda_\sigma = 0.71$, and $\lambda_n = 1.007$. In contrast, the blip function method, which assumes $\lambda_n = 1$, determines in this case the value $\lambda_\sigma = 1.209$ and the unphysical HS volume fraction $\phi_{HS} = 2.41$.

Finally, Fig. (3c) reports the same exercise but for a much softer and longer-ranged interaction, namely, the HSY liquid with $K = 554$, $z = 0.149$, and $\phi = 2.8\times10^{-3}$. As before, the solid line is the RDF of the equivalent HS system as a function of r/σ_{HS}. In this case, the resulting effective HS parameters are $\phi_{HS} = 0.49$, $\sigma_{HS}/\sigma = 5.55$, and $n_{HS}/n = 1.015$, leading to the overall agreement between RDFs shown in the figure. In this case the blip function method ($\lambda_n = n_{HS}/n = 1$) determines the completely unphysical values $\lambda_\sigma = \sigma_{HS}/\sigma = 27.6$ and $\phi_{HS} = 63.4$. Thus, the first conclusion of these three illustrative examples is that the assumption that $\lambda_n \approx 1$, employed in the blip function method above, is indeed a very good assumption, at least for these three potentials at the states structurally corresponding to the HS liquid at $\phi_{HS} = 0.49$. It is then the determination of the hard sphere diameter through Eq. (19) what should be avoided, and substituted by the procedure illustrated in our examples.

Let us mention that in each of the three cases corresponding to panels (a)-(c) of Fig. (3) we chose to plot the two equivalent RDFs as a function of the radial distance r measured in the length unit σ of the respective system. This comparison, however, can also be done using instead the effective HS diameter σ_{HS} as the common unit length, as it is done in Fig. (3d). There we note, in addition, that the simulation data of the three systems are actually coincident, and that we only have a single HS RDF, corresponding to $\phi_{HS} = 0.49$ and represented by the only solid line in the figure. This coincidence illustrates another important feature, namely, that different soft-sphere systems that share the same effective HS volume fraction also share the same static structure.

This figure also illustrates the fact that the structural equivalence condition in Eq. (13) can also be used in an inverse manner, i.e., to identify the state of a given soft-sphere system whose structure matches the structure of a prescribed HS system. In reality, what we actually did for each of the three soft-sphere model systems in the examples in Fig. (3) was to search for the state whose structure matched the structure of the HS liquid with the prescribed volume fraction $\phi_{HS} = 0.49$. For this we varied the soft-sphere density (or volume fraction ϕ), keeping the temperature fixed at $T^* = 1$, until meeting this condition.

Another important observation is that for the model interaction potentials employed in the present discussion, the height of the second maximum of the RDF is not the only simple structural order parameter. In reality, some other properties that derive from the general equivalence

condition in Eq. (13) might serve as alternative structural order parameters. One of them is the main peak of the static structure factor $S(k)$, whose height S_{max} allows us to determine ϕ_{HS}, and whose rescaled position k_{max} determines the effective HS diameter σ_{HS}, as illustrated in Fig. (4), which exhibits the structure factors of the same systems as in the previous figure, plotted as a function, in one case of $k\sigma$ (insets) and in the other case of $k\sigma_{HS}$ (main figure).

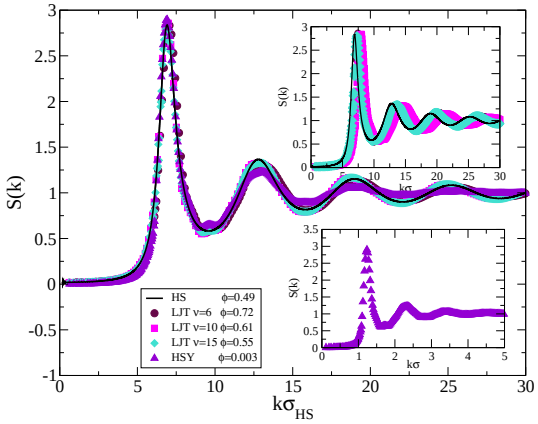

FIG. 4: Structure factors for the TLJ and Yukawa systems with effective volume fraction $\phi_{HS} = 0.49$.

Since our study will extend to densities higher than the freezing density of the monodisperse fluid, to study the metastable states we need to introduce polydispersity in our simulation. Although this will not affect dramatically the most relevant dynamic properties, it happens to have a profound effect on the thermodynamic and structural properties, in particular on the height of the second peak of $g(r)$ and of the main peak of $S(k)$. These structural order parameters are found to decrease with polydispersity (for fixed volume fraction), and this requires us to adapt the method described above, to identify in a simple manner the effective hard-sphere system that corresponds to a given *polydisperse* soft-sphere liquid. The adapted procedure is the following. Consider a given soft-sphere system with (size) polydispersity P and mean diameter σ, whose RDF $g(r/\sigma; \phi, T^*, \nu)$ has been measured or simulated. We then model its equivalent hard-sphere system with the same polydispersity P as an equi-molar binary mixture of hard spheres of mean HS diameter σ_{HS} and total volume fraction ϕ_{HS} whose overall RDF $g_{HS}(r)$ ($\equiv [g_{11} + 2g_{12} + g_{22}]/2$, with $g_{\alpha\beta}$ being the partial radial distribution functions) are obtained from the analytic solution of the *multicomponent* Percus-Yevick approximation [43, 44], complemented again with the VW correction (i.e., Eqs. (9)-(12) with σ and ϕ reading σ_{HS} and ϕ_{HS}, denoted as PY-VW). As in the monocomponent case, the resulting RDF $g_{HS}(r)$ is then compared with the simulation results to extract the value of ϕ_{HS} that matches the height of the second peak of the RDF.

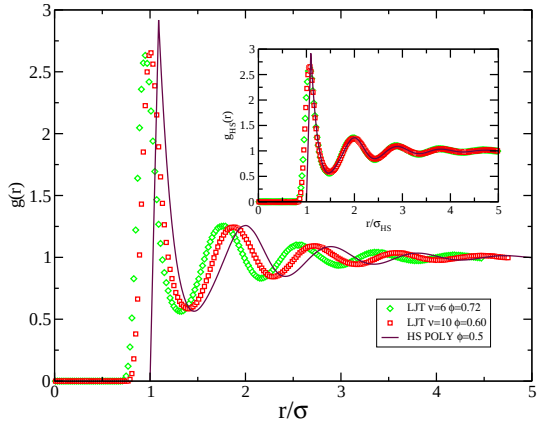

FIG. 5: Simulated radial distribution function $g(r)$ for polydisperse systems with polydispersity $P = 0.0866$. In the main panel we present the results for TLJ systems (symbols) with $\nu = 6$ and $\nu = 15$, for $\phi_{HS} = 0.5$. The lines correspond to the solutions of the PY-VW theory for the corresponding HS systems. Inset: RDFs after scaling the radial distance.

We illustrate this structural equivalence using a polydisperse version of the TLJ model with different softness, $\nu = 6$ and $\nu = 15$, but with densities corresponding to the same effective HS volume fraction $\phi_{HS} = 0.5$, and the same polydispersity $P = 0.0866$ (which is large enough to inhibit the crystallization of hard spheres up to very high volume fractions [38]). Figure (5) presents the simulation results, along with the theoretical data for the corresponding binary mixtures. We see here that the scenario depicted in the insets is quite similar to the one for monodisperse systems. Furthermore, the scaling of the radial distance with the effective HS diameter renders the structure of the systems to collapse onto each other, as it can be appreciated in the main figure. Thus, the results in Figs. (3) and (5) show that our protocol to extract the equivalent hard sphere system works very well in a wide range of volume fractions for both monodisperse and polydisperse systems. With this essential step covered, we now investigate its implications on the dynamics of the equivalent systems.

SOFT-HARD DYNAMIC EQUIVALENCE

The *dynamic* extension of the previous soft–hard static structural equivalence was discussed in Refs. [26, 42] in the context of the dynamics of Brownian liquids, in which a short-time self-diffusion coefficient D^0 describes the diffusive microscopic dynamics of the colloidal particles "between collisions". The following discussion also refers to Brownian systems, but in the second part of this section we shall consider atomic liquids, whose short-time dynamics is ballistic.

Dynamic equivalence in Brownian liquids

Although the dynamic equivalence we are about to discuss can probably be understood from several perspectives, in our case we view it as a straightforward prediction of the self-consistent generalized Langevin equation (SCGLE) theory of colloid dynamics and dynamic arrest. This theory can be summarized by a closed system of equations for the collective and self intermediate scattering functions $F(k,t)$ and $F_S(k,t)$ [21–23], which in Laplace space read

$$F(k,z) = \frac{S(k)}{z + \frac{k^2 D^0 S^{-1}(k)}{1+m(k)\Delta\zeta^*(z)}}, \tag{21}$$

and

$$F_S(k,z) = \frac{1}{z + \frac{k^2 D^0}{1+m(k)\Delta\zeta^*(z)}}, \tag{22}$$

with D^0 being the short-time self-diffusion coefficient. These equations become a closed system of equations when complemented with the following approximate expression for the time-dependent friction function $\Delta\zeta^*(t)$,

$$\Delta\zeta^*(t) = \frac{D^0}{3\,(2\pi)^3\, n} \int d\mathbf{k} \left[\frac{k[S(k)-1]}{S(k)}\right]^2 F(k,t) F_S(k,t), \tag{23}$$

and with the following definition of the "interpolating" function $m(k)$ [23]

$$m(k) \equiv \frac{1}{1+\left(\frac{k}{k_c}\right)^{\mu}}, \tag{24}$$

with $\mu = 2$ and with k_c being the empirically chosen cutoff wave-vector $k_c = 8.2/\sigma$.

From the condition for structural equivalence in Eq. (13), $g\,(r/\sigma;\phi,T^*,\nu) \approx g_{HS}(r/\sigma_{HS};\phi_{HS})$ and assuming that $\lambda_n = n_{HS}/n = 1$ (an excellent assumption in the present case), it is not difficult to see that the dimensionless properties $F(k,t)$, $F_S(k,t)$, and $\Delta\zeta^*(z)$ of a given soft-sphere system, can only depend on the wave-vector k and the time t through the dimensionless variables $k^* \equiv k\sigma_{HS}$ and $t^* \equiv D^0 t/\sigma_{HS}^2$, and that the previous equations become identical to those of the hard-sphere system at volume fraction ϕ_{HS}. This is the origin of the predicted dynamic equivalence, summarized by the statement that the dynamic properties of the fluid with soft repulsive potential $u(r)$, such as the self intermediate scattering function (self-ISF) $F_S(k,t;n,T;\sigma,\epsilon,\nu;D^0)$, can be approximated by the corresponding property of the (statically) equivalent hard-sphere Brownian liquid whose particles diffuse with the same D^0, i.e., $F_S(k,t;n,T;\sigma,\epsilon,\nu;D^0) \approx F_S^{(HS)}(k,t;n,\sigma_{HS};D^0)$. This relationship can be written in terms of dimensionless variables as $F_S(k\sigma,D^0t/\sigma^2;\phi,T^*,\nu) \approx F_S^{(HS)}(k\sigma_{HS},D^0t/\sigma_{HS}^2;\phi_{HS})$, or

$$F_S(k\sigma,D^0t/\sigma^2;\phi,T^*,\nu) \approx F_S^{(HS)}(\lambda_\sigma k\sigma,\lambda_\sigma^{-2}D^0t/\sigma;\lambda_\sigma^3\phi), \tag{25}$$

with λ_σ defined in Eq. (15). Some consequences of the universality summarized by Eq. (25) were illustrated in Refs. [26] and [42] in the context of the TLJ potential. Those references, however, discussed in detail only the limit of moderate softness ($\nu \gg 1$), in which the strong similarity with the HS potential leads to the additional simplification that $\sigma_{HS}(n,T,\nu)$ becomes n-independent, and given by the "blip function" approximation [26, 29]. These, however, are actually unessential restrictions, and to illustrate this we have performed Brownian dynamics simulations for the non-truncated IPL and HSY models.

The universality summarized by Eq. (25) leads to the corresponding scaling rules for other properties. For example, let

$$W(t;T^*,\phi,\nu) \equiv <(\Delta\mathbf{r}(t))^2>/6 \tag{26}$$

be the mean squared displacement of any soft-sphere liquid at a given state (T^*,ϕ,ν) that structurally maps onto the hard-sphere liquid of diameter $\sigma_{HS}(T^*,\phi,\nu)$ and volume fraction $\phi_{HS}(T^*,\phi,\nu)$. Then the normalized MSD

$$W^*(t^*;T^*,\phi,\nu) \equiv <(\Delta\mathbf{r}(t^*))^2>/6\sigma_{HS}^2(T^*,\phi,\nu), \tag{27}$$

with $t^* \equiv D^0t/\sigma_{HS}^2$, will be identical to that of the equivalent hard-sphere fluid,

$$W^*(t^*;T^*,\phi,\nu) = W_{HS}^*[t^*;\phi_{HS}(T^*,\phi,\nu)], \tag{28}$$

and for that matter, to that of any other soft-sphere liquid that is structurally equivalent to the HS system with the same volume fraction ϕ_{HS}.

To test this prediction in Fig. (6) we present the BD results for the mean squared displacement of the three soft-sphere systems discussed in Fig. (3) (i.e., the TLJ with $\nu = 6$, the IPL with $\nu = 3$, and the HSY with $K = 554$ and $z = 0.149$), all of them corresponding to an equivalent volume fraction $\phi_{HS} \approx 0.49$. The MSD is presented in the figure in the natural units of the simulations, i.e. as $[W(t)/\sigma^2]$ vs. $[D^0t/\sigma^2]$. We observe that the MSD exhibits the two linear regimes typical of Brownian systems [45]: at short times $[W(t)/\sigma^2] \approx [D^0t/\sigma^2]$ whereas at long times $[W(t)/\sigma^2] \approx D^*[D^0t/\sigma^2]$, where $D^* \equiv D_L/D^0$ is the long-time self-diffusion coefficient D_L scaled with D^0. Thus, at short times the MSD must be the same for all systems and states, a condition clearly fulfilled by the data plotted in the figure.

In the long-time regime, on the other hand, $[W(t)/\sigma^2]$ is proportional to the scaled long-time self-diffusion coefficient D^*, which does depend on the interparticle interactions, and hence, on the particular system and on its state (T^*, ϕ, ν). Thus, the various $W(t)$ in Fig. (3) should differ in their long-time behavior. They, however, exhibit the same long-time limit. The reason for this is another scaling that derives from the dynamic equivalence condition in Eq. (25), namely, that the dimensionless parameter D^* depends on (T^*, ϕ, ν) only through the effective HS volume fraction $\phi_{HS} = \phi_{HS}(T^*, \phi, \nu)$,

$$D^*(T^*, \phi, \nu) \approx D^*_{HS}[\phi_{HS}(T^*, \phi, \nu)]. \qquad (29)$$

Since the three systems in this figure were chosen to have the same ϕ_{HS} $(= 0.49)$, they must share the same value of D^* (≈ 0.1). According to the scaling indicated in Eq. (28), however, the three systems in Fig. (3) must share the same $W^*(t^*)$, i.e., the three different MSDs in the figure should collapse onto the same curve when plotted as a function of $t^* \equiv D^0 t/\sigma^2_{HS}$. This is indeed what we find, as illustrated in the inset of Fig. (6), which shows that the results corresponding to the three curves of the main panel do collapse onto each other when plotted in this scaled manner. According to Eq. (28), the resulting master curve then determines exactly the function $W^*_{HS}[t^*; \phi = 0.49]$. The SCGLE theory, besides predicting this scaling also provides an approximate prediction for this function. This prediction is represented by the dashed line in the inset of Fig. (6), which we see follows closely the simulations results.

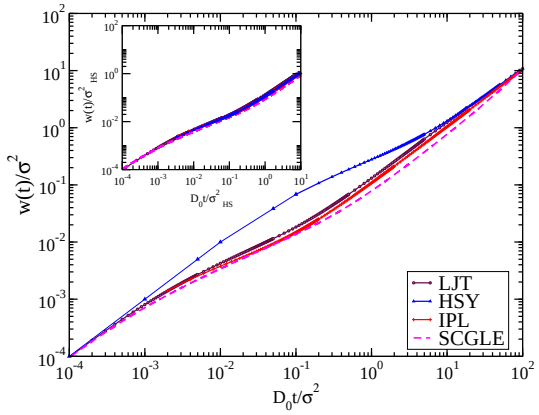

FIG. 6: BD results for the mean squared displacement $W(t)$ for TLJ $(\nu = 6)$, IPL $(\nu = 3)$, and HSY $(K = 554,\ z = 0.149)$ systems with the same effective volume fraction $\phi_{HS} = 0.49$. Inset: Results scaled in HS units. The dashed line corresponds to the predictions from the SCGLE theory for HS system.

The results presented in the figure are concerned with the full MSD at the single volume fraction $\phi_{HS} = 0.49$. We now extend our study to other volume fractions, paying special attention to long-time properties such as the long-time diffusion coefficient D_L and the α-relaxation time τ_α. We start by presenting in Fig. (7a) the BD results for $D^* = D_L/D^0$ (in the format $1/D^*$), as a function of ϕ, for several soft-sphere systems. The main panel of the figure, which includes TLJ systems and the solution to the SCGLE theory for Brownian systems (i.e., Eqs. (21)-(24)) applied to the HS fluids, clearly shows how the simulated D^* depends on volume fraction and softness. For instance, D^* is, as expected, a decreasing function of ϕ and ν. It is also apparent in the figure that D^* steadily approaches the SCGLE HS results as the potential becomes stiffer. In particular, all the results in the figure converge in the low-ϕ limit to the correct limiting value $D^*(\phi \to 0) = 1$.

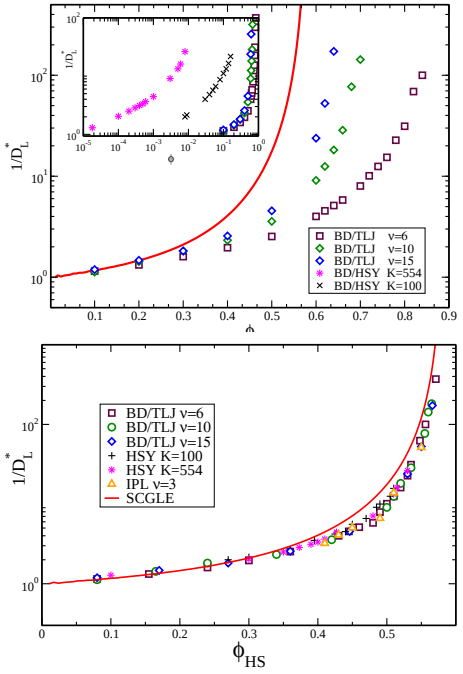

FIG. 7: (a) Scaled long-time diffusion coefficient $D^* = D_L/D^0$ from DB simulations for TLJ systems with $\nu = 6$, $\nu = 10$ and $\nu = 15$, at different volume fractions ϕ. Inset: Results that include the two HSY systems with $K = 554$, $z = 0.149$, and $K = 100$ $z = 1.0$. (b) Results plotted as a function of the effective volume fraction ϕ_{HS}. The solid line represents the solution for HS systems from the colloidal SCGLE theory.

Depending on the specifics of the interaction potential, other model systems can depart even further from the theoretical results. In the inset of Fig. (7a), for instance, where we compare the data in the main panel with the results for two HSY monodisperse systems, the difference with theory and short ranged systems is clear. Here the values of D^* in the liquid regime are covered by the HSY systems for volume fractions in the range $10^{-5} - 10^{-1}$ (from weakly to highly structured condi-

tions), whereas the volume fractions of the TLJ systems fall in the typical range $0.1 \lesssim \phi \lesssim 1$. Despite these differences, however, when the data are plotted as suggested by the scaling in Eq. (29), see Fig. (7b), all the data fall on a well-defined master curve, which must coincide with the exact hard-sphere function $D^*_{HS}[\phi]$. In fact, an approximation to this function is provided by the SCGLE theory, which is represented by the solid line in the figure. Let us notice that, although the results in the figure illustrate the dynamic equivalence at the very particular condition $t \to \infty$, basically the same scaling holds at all times for time-dependent properties such as the scaled time-dependent self-diffusion coefficient $D^*(t) \equiv W(t)/6D^0t$ (illustrated in Fig. (4) of Ref. [42])) or the scaled MSD $W^*(t)$ (illustrated here in Fig. (6)).

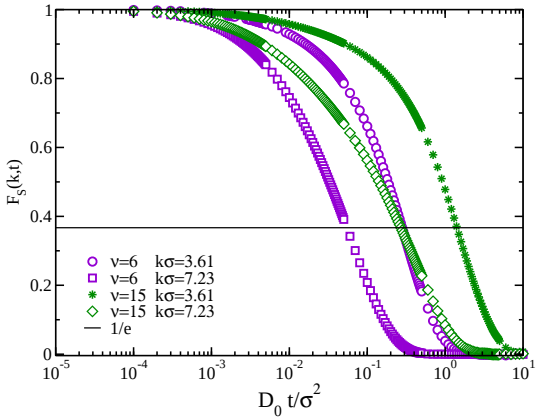

FIG. 8: Self-intermediate scattering function $F_S(k,t)$ from BD simulations for TLJ systems with $\nu = 6$ and $\nu = 15$, at the volume fraction $\phi = 0.6$. Results are presented for two wave vectors k_1 and k_2, with $k_1 < k_2$. The solid horizontal line represents the target value $F_S = 1/e$ that identifies the α-relaxation time τ_α of the systems.

We now turn our attention to the relaxation of the correlation function $F_S(k,t)$. This is a function that depends on the parameters of the system, like the volume fraction ϕ, the wave vector k, and the softness of the potential. In Fig. (8) we illustrate some of its features by plotting results for a TLJ system with $\phi = 0.6$, for two values of the softness parameter, $\nu = 6$ and $\nu = 15$, and two wave vectors, $k_1\sigma = 3.61$ and $k_2\sigma = 7.23$. The solid horizontal line represents the target value $F_S(k,\tau_\alpha) = 1/e$, which identifies the α-relaxation time τ_α of the systems. The data in the figure shows that, for ν fixed, $F_S(k,t)$ relaxes faster with the larger wave vector. The other feature to notice is that, for a given value of k, $F_S(k,t)$ decays faster for the softer system (i.e., for $\nu = 6$), although the very initial evolution is rather similar for the two systems. This behavior is expected because the effective excluded volume of TLJ systems decreases with the softness of the potential, and therefore the structural relaxation is faster for softer systems.

Since the choice for k is not unique, in this work we use

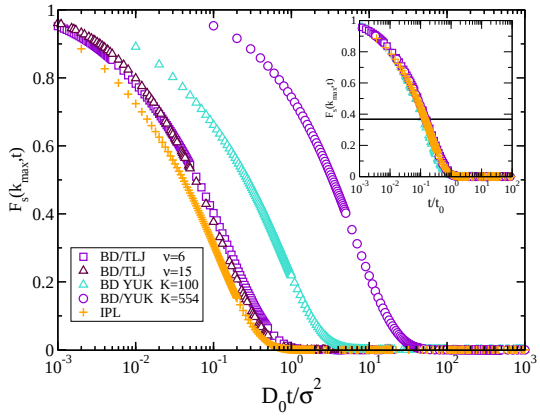

FIG. 9: Self-intermediate scattering function $F_s(k_{max},t)$ from BD simulations for TLJ systems with $\nu = 6$, $\nu = 10$ and $\nu = 15$, and for a Yukawa system with $K = 554$ and $z = 0.149$. All systems have an effective volume fraction $\phi_{HS} = 0.49$. In the inset the results presented with time scaled according to $t \to \lambda_\sigma^{-2}t$.

$k = k_{max}$, the position of the main peak of the structure factor. In this way structurally equivalent systems will then be explored with the same dominant wave vector in the hard units, $\lambda_\sigma k_{max}\sigma$, as indicated by the results presented in Fig. (4). We evaluate then $F_S(k_{max},t)$ for two TLJ and one HSY systems with equivalent volume fraction $\phi_{HS} = 0.49$ and the same potential parameter σ, and plot the results in Fig. (9) as a function of the scaled time D^0t/σ^2. In such units, the figure shows that the TLJ and HSY systems differ notoriously. In particular, the α-relaxation time between the two types of systems differs by more than a decade, despite the underlying iso-structurality between the systems, reflecting the influence of the potentials on dynamic properties of the systems. Dynamic equivalence, as indicated by Eq. (25), should however lead to a collapse of all the curves upon the transformation to HS units. That this is the case is shown in the inset of the figure, where the collapse of the curves is achieved by by plotting the data as a function of the time scaled not as D^0t/σ^2, but as D^0t/σ^2_{HS}, as suggested by Eq. (25). Note here that the other conditions on the wave vector and the volume fraction implied by that equation are already fulfilled because all the systems share the same effective volume fraction. Such scaling of F_S in turn implies that the α-relaxation time τ_α, a particularly important dynamic property in high density or low temperature liquids, turns out to be the same for iso-structural systems when expressed in units of the equivalent HS system, regardless of the softness of the interaction between the particles.

By performing BD simulations at different volume fractions we are able to extract the α-relaxation time as a function of ϕ. In the main panel of Fig.(10), where only the TLJ systems are presented, τ_α exhibits the typical trends found in liquids; it is small for low and moder-

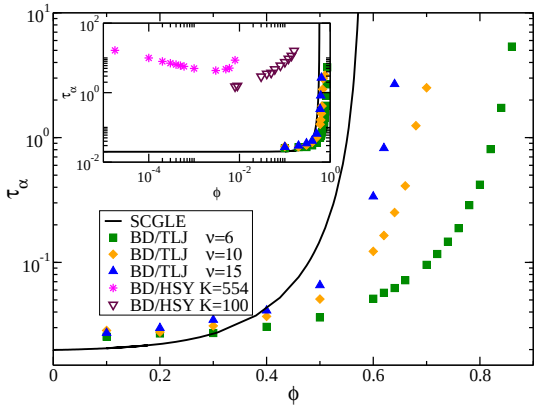

FIG. 10: α-relaxation time τ_α, in BD units, for TLJ and HSY systems at different volume fractions. The figure includes the corresponding results for HS systems from the SCGLE theory (solid line). Inset: Results that include two HSY systems, one with $K = 554$ and $z = 0.149$, and the other with $K = 100$ and $z = 1.0$.

ate volume fractions, and then increases rapidly at a rate that depends strongly on the softness of the potential, especilly at high volume fractions, as it can be seen in the figure. For example, taking as a reference the line $\tau_\alpha/t_{BD} = 1$, the volume fractions reach the approximate values $\phi = 0.57, 0.61, 0.77$ for $\nu = 15, 10, 6$, respectively. Overall, increasing ν leads the results progressively close to those of HS systems predicted by the SCGLE theory, which in the figure are represented by the solid line.

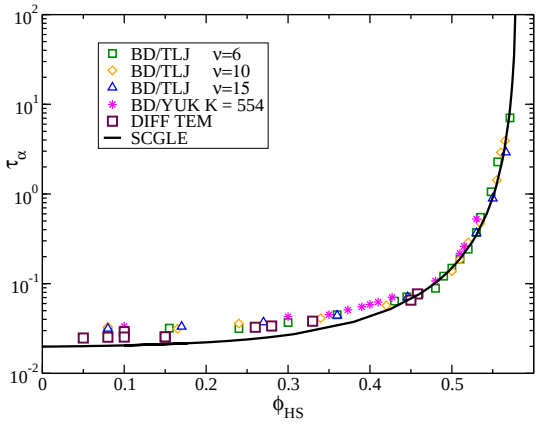

FIG. 11: α-relaxation time τ_α in HS units. The solid line corresponds to the results from the SCGLE theory applied to HS fluids.

In the inset of the figure we replot the results in the main panel along with those for two HSY systems. This inset then allows us to compare directly the α-relaxation time between systems with rather different potentials both in range and strength. As expected, the difference between HSY and TLJ systems is rather significant, but largely dependent on the screening and the strength of the HSY potential. Thus, although τ_α is haighly sensitive to the volume fraction and the conditions of the interaction potential, the scaling properties of $F_S(k,t)$ already illustrated in Fig. (9) should translate to τ_α and make the data in the current figure aling with those of equivalent HS systems. To corroborate this we apply the scaling rules for time and volume fraction provided before, i.e. we transform the data according to $\phi \to \phi_{HS} = \lambda_\sigma^3 \phi$ and $[\tau_\alpha]_{BD} = \tau_\alpha/t_{BD} \to [\tau_\alpha]_{HS} = \lambda_\sigma^{-2}[\tau_\alpha]_{BD}$, where $t_{BD} = \sigma^2/D^0$ is the time unit in DB simulations. The final results are plotted in Fig. (11), where we can appreciate that the applied transformations work very well, collapsing all the data onto a single curve. Note that the transformed data follows closely the solid line, i.e., the SCGLE theoretical predictions for HS fluids.

Dynamic equivalence in atomic liquids

In recent work, our group has extended the colloidal SCGLE theory to the domain of atomic liquids. There, it has been found that the overdamped colloidal equations for $F(k,z)$, $F_S(k,z)$, and $\Delta\zeta(t)$, i.e., Eqs. (21), (22), and (23) are formally equivalent to those of atomic systems, subjected to a reinterpretation of the difusion coefficient D^0, which in the atomic case depends on density and temperature. This formal identity then implies that the Newtonian liquids with the same $S(k)$ should exhibit soft-hard dynamic equivalence in the same way as Brownian colloids. In particular, the universality expressed in Eqs. (25), (27) and (29) are then extended to molecular fluids. Note that such equations are written in terms of the scaled time t/t_{BD}, with $t_{BD} = \sigma^2/D^0$, i.e., in terms of the short time property D^0. Thus, even though the same applies to the atomic case, with the corresponding interpretacion of D^0, we can choose instead to scale the atomic equations with the natural short-time scale of Newtonian dynamics, which is $t_{MD} = \sqrt{M\sigma^2/k_BT}$, thus bypassing the explicit form of D^0 for atomic liquids. The use of t_{MD} as the time scale leads to a different scaling rule when transforming to HS units. In this case, time is now tranformed as $t_{HS} = \lambda_\sigma t_{MD}$, which contrast with the Brownian case where $t_{HS} = \lambda_\sigma^2 t_{BD}$.

In what follows, we employ t_{MD} and the corresponding expresion for t_{HD} to study the dynamic equivalence between soft-sphere and hard-sphere atomic fluids. It should be noted, however, that the static structure of our soft systems depends on the volume fraction and the specifics of the parameters of the potential, but not on the underlying dynamics, it being Brownian or Newtonian. As such, the structure factor or the pair correlation function of a given system, when simulated with BD, is identical to that obtained through MD simulations. In particular, then, the soft-hard static structure equivalence stated by equations (13) or (17) will still be valid for Newtonian fluids, which allows us to discuss the soft-hard dynamic equivalence of atomic liquids in the

context of iso-structural systems.

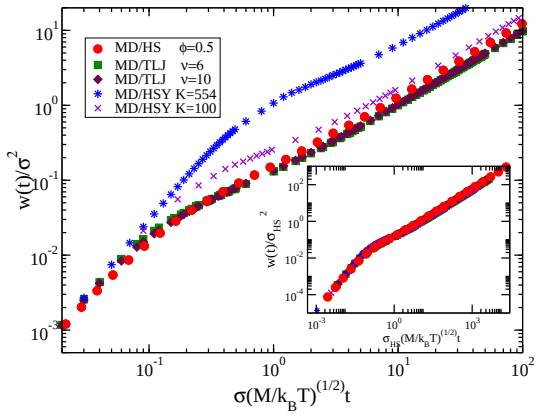

FIG. 12: Mean squared displacement from molecular dynamics simulations for iso-structural soft systems with equivalent $\phi_{HS} = 0.49$. The filled circles correspond to the MD simulations of a HS fluid. The results are presented in units of σ and t_{MD}. Inset: MSDs after transforming to HS units.

share a common long-time diffusion coefficient D_L, which is defined as the limit $D_L(\phi) = \lim_{t\to\infty} W(t)/t$.

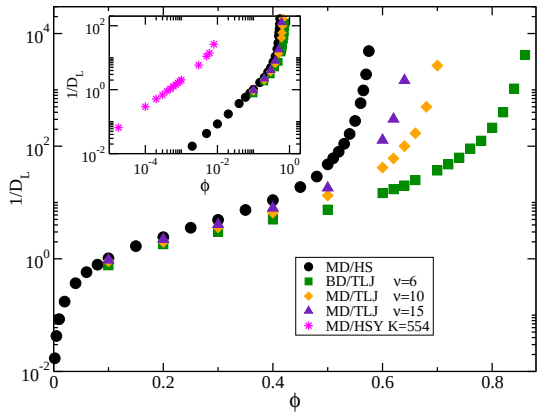

FIG. 13: Scaled diffusion coefficient $D_L^*(\phi) = D_L(\phi)/(\sigma^2/t_{MD})$ from MD simulations for several soft systems. Inset: Results that include the HSY system with $K = 554$ and $z = 0.149$. The filled circles correspond to HS systems.

We begin by presenting MD results for the MSD for some of our working systems, namely, a TLJ system with $\nu = 6$ and 15, a HSY system with $K = 554$, $z = 0.149$, and an IPL system with $\nu = 3$, all of them at the effective volume fraction $\phi_{HS} = 0.49$; at the same time, we include the corresponding data for the hard spheres fluid, from event-driven MD simulations. The MSD for these cases are presented in Fig. (12), where all quantities are scaled according to the MD units σ and $t_{MD} = (M\sigma^2/k_BT)^{1/2}$. The systems in the figure clearly display the two linear regimes, ballistic and diffusive, characteristic of Newtonian systems, with the HSY system departing more strongly from the exact results (the HS data). Although all the systems follow the same curve at short times, the HSY system takes longer to cross the ballistic-to-diffusive transition, leading to larger values in the MSD at a given time. In fact, we have found that our systems follow an specific trend depending on the type of potential. We have found that, at long times, the MSD of long-ranged systems (HSY and IPL) are always above the HS data, whereas short-ranged systems (i.e. for TLJ) are always below and systematically approaching the exact results as the potential becomes stiffer.

The MSD of these iso-structural systems can be made to coincide when plotted in HS units. As before, the MSDs are transformed according to equation (28), with time scaled in a different manner to reflect the underlying Newtonian dynamics of the systems. In the present case, the transformation $\sigma \to \sigma_{HS}$ leads to $t^* = t/t_{MD} \to \lambda_\sigma^{-1} t^*$, from which we get $\lambda_\sigma^2 W(\lambda_\sigma^{-1} t^*)$. By scaling in this manner we appreciate in the inset of the figure that all the systems follow nicely the results for the HS system. Then we see that all the soft, iso-structural systems have the same ballistic and diffusive regimes, and in particular

The dependence of $D_L(\phi)$ on the volume fraction and the model interaction is now presented in figure (13) in the units of the simulation. i.e., as $D_L^* = D_L/(\sigma^2/t_{MD})$. The main panel is dedicated to TLJ systems, whereas the inset centers on the marked contrast between the strongly repulsive, long-ranged HSY system with $K = 554$ with other soft systems, particularly TLJ. Overall, we find that the data for mid and high volume fractions exhibits similar trends to those already observed in DB simulations of TLJ systems. The contrast between HSY and the other soft systems shown in the inset is also similar. The main qualitative difference between MD and DB can be observed at low volume fractions, where BD approaches the limiting condition $D^*(\phi \to 0) \to 1$ due to the diffusive nature of its short-time dynamics, whereas D_L^* from MD increases sharply ($1/D_L^*$ goes to zero) as the volume fraction decreases. In the latter case the Newtonian particles perform ballistic motion most of the time, with a collision rate that decreases as the system becomes more dilute. In fact, the correct ϕ-dependence of D_L^* for dilute Newtonian fluids can be obtained from kinetic theory as $D_L^* \sim 1/\phi$ [49], which explains the shape of the data at low ϕ.

Figure (14) summarizes the results for the diffusion coefficient for a variety of soft-repulsive systems (including those in the previous figure), now in units of the equivalent HS systems. In this case, the applied transformation is $D_L \to D_L^{HS} = \lambda_\sigma D_L^*$. Note that we plot $1/D_L^{HS}$ and D_L^{HS} to better appreciate that results at both low and high volume fractions. From these two forms of the results we see clearly that this long-time dynamic property, D_L, obtained through the simulation of a variety of repulsive systems, follows very well the corresponding data for truly hard spheres in all the range of volume fractions

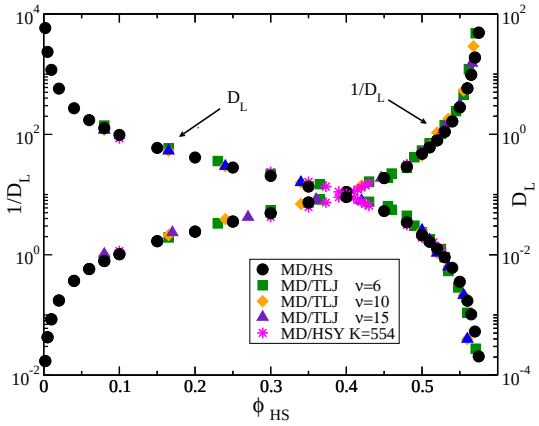

FIG. 14: Long-time diffusion coefficient D_L^*, in HS units, as a function of the effective HS volume fraction of the systems. The left vertical axis presents $1/D_L^*$, and the right vertical axis D_L^*.

considered in the figure.

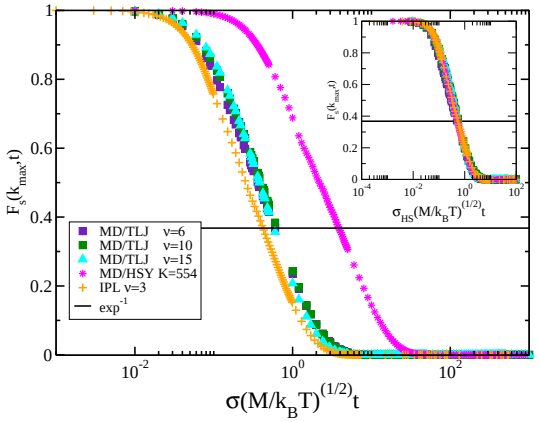

FIG. 15: Correlation function $F_S(k_{max},t)$ from MD simulations for TLJ ($\nu = 6, 15$), IPL ($\nu = 3$), and HSY ($K = 554$) systems with the same equivalent volume fraction $\phi_{HS} = 0.49$. Time is in units of $t_0 = t_{MD}$. Inset: Results after transforming to hard units via $t_0 = \lambda_\sigma t_{MD}$. The horizontal line represents the value $F_S(k_{max}, t = \tau_\alpha) = 1/e$.

In what follows we now focus on the properties of the atomic self-ISF. As before, the behavior of $F_S(k,t)$ is first investigated to show the its principal trends under different soft model systems. Later we focus on the long time behaviour through the α-relaxation time. Following our previous analysis for $F_S(k,t)$, this function is studied at $k = k_{max}$ for several disimilar interaction potentials. Thus, in figure (15) we present $F_S(k_{max},t)$ for iso-structural systems, with time and wave vector in MD units. The figure includes results for TLJ ($\nu = 6$ and $\nu = 15$), IPL ($\nu = 3$), and HSY ($K = 554$) systems, all of them with equivalent volume fraction $\phi_{HS} = 0.49$. As we can see, the scenario is rather similar to that of Brownian fluids, with the results for TLJ and ILP potentials very close to each other, but far from those corresponding to the HSY potential. More importantly, the figure also shows that the $F_S(k_{max},t)$ of iso-structural systems can be made to fall on top of each other upon transforming to HS units. This is illustrated in the inset, where we plot the data in the main panel in the scaled form $F_S(\lambda_\sigma k^*_{max}, \lambda_\sigma^{-1} t^*)$, where k^*_{max} and t^* are the wave vector and time in MD units. This result, along with the universality expressed by Eq. (25), indicates that the master curve followed by the systems corresponds to the one followed by a Newtonian hard-sphere system at the effective volume fraction shared by all the systems, $\phi_{HS} = 0.49$.

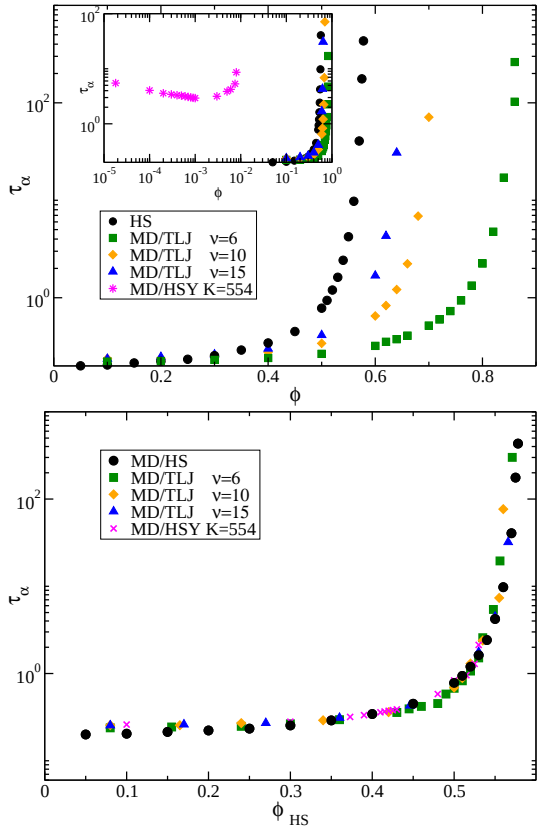

FIG. 16: (a) α-relaxation time as a function of the volume fraction, $\tau_\alpha(\phi)$, for selected TLJ, IPL, and HSY systems. The filled circles represent the results for HS systems. Inset: Results that include two HSY systems, one with $K = 554$ and $z = 0.149$, and the other with $K = 100$ and $z = 1.0$. (b) $\tau_\alpha(\phi)$ in HS units.

The above results for $F_S(k,t)$ were presented for iso-structural systems at a single value of the equivalent hard-sphere volume fraction. Now we address its potential and volume fraction dependence, as well as to its scaling properties, not through $F_S(k,t)$ itself, but through its long-time characteristic property τ_α. To this end, in Fig. (16a) we present the α-relaxation time, as a function of the volume fraction, for selected soft systems. The main panel is dedicated to the softness of the

TLJ potential. We observe here that the general trends in terms ν and ϕ resemble closely those of Brownian systems previously disscussed. In the inset, where HSY and TLJ systems are constrasted, we find that the HSY fluids deviate strongly from the TLJ systems, especially for the stronger potential ($K = 554$ and $z = 0.149$), a similar trend found for Brownian systems. The results plotted in Fig. (16b) represent the α-relaxation time for a collection of soft systems after transforming to HS units, i.e., the volume fraction as $\phi \to \phi_{HS}$ and the relaxation time as $\tau_\alpha/t_{MD} \to \lambda_\sigma \tau_\alpha/t_{MD}$. The results in this figure shows that the transformation to hard units works very well and that the soft systems follow nicely the MD data of strictly hard spheres (black symbols).

BROWNIAN-ATOMIC DYNAMIC EQUIVALENCE

As mentioned above, our group has extended the SCGLE theory to atomic liquids. There, the overdamped or long-time limit of the equations for $F(k,t)$, $F_S(k,t)$, and $\Delta\zeta(t)$, equations (21), (22), and (23), have been found to be formally equivalent for both colloid and atomic fluids, the fundamental difference being the definition of the diffusion coefficient D^0. In colloid liquids D^0 is a constant, identical to the short-time self-diffusion coefficient given, for example, by the EinsteinStokes expression in the absence of hydrodynamic interactions. In the atomic case, on the other hand, D^0 depends on temperature and density, and is given by the kinetic-theoretical result [49]

$$D^0 = D^0(\phi) = \frac{3}{8\sqrt{\pi}} \left(\frac{k_B T}{M}\right)^{1/2} \left(\frac{1}{n\sigma^2}\right) \qquad (30)$$

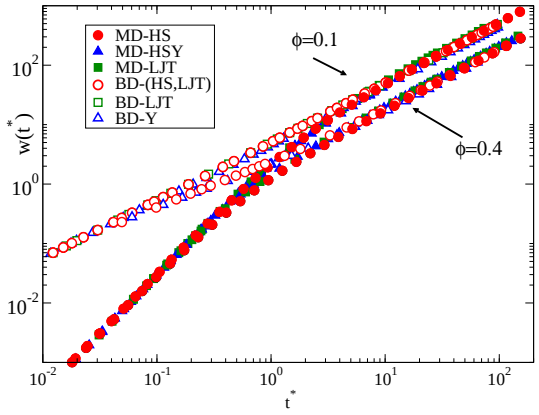

FIG. 17: Scaled mean squared displacement, simulated with molecular dynamics (MD, solid symbols) and Brownian dynamics (BD, empty symbols) for fluids with hard-sphere (HS, circles), truncated Lennard-Jones (TLJ, squares) and repulsive Yukawa (Y, trian- gles) interactions, for states corresponding to $\phi_{HS} = 0.1$ and 0.4.

Thus, this formal identity implies that the long-time dynamic properties of an atomic liquid will then coincide with the corresponding properties of a colloidal system with the same $S(k)$, provided that the time is scaled as $D^0 t$, with the respective meaning and definition of D^0. One example of such long-time properties is the long-time self-diffusion coefficient D_L, which in scaled form is $D^* = D_L/D_0 \lim_{\to\infty} W(t)/D_0 t$, is predicted to be indistinguishable for atomic and Brownian systems. This colloidal-atomic dynamic correspondence was illustrated in Fig. (2) of the reference (which we reproduce here in Fig. (17)) for some iso-structural systems at the volume fractions $\phi_{HS} = 0.1$ and 0.4.

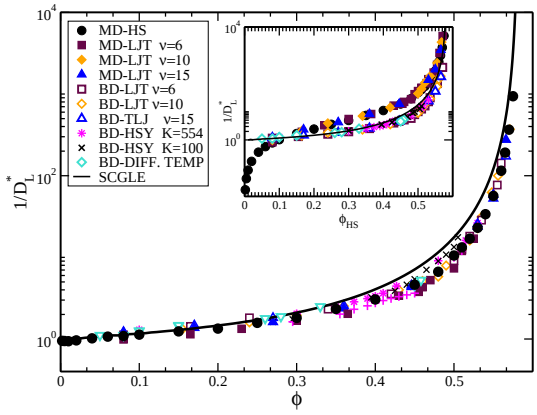

FIG. 18: Long time diffusion coefficient for colloid and atomic liquids. In the main panel $D_L(\phi)$ is plotted in the corresponding units, i.e., in DB or MD units. Inset: Scaled results.

This colloidal-atomic dynamic correspondence extends over to HS systems and systems with soft repulsive interactions. We illustrate this in Fig. (18), where we plot the long-time diffusion coefficient $D_L(\phi)$ for a wide range of interacting conditions. The inset of the figure, for instance, we plot again our previous results for D_L from MD and BD simulations, scaled according to their transformation rules. There, one can appreciate the fundamental differences between the two types of dynamics (colloid and atomic) when presented in the equivalent HS units. The main panel, on the other hand, present all those results after scaling the difussion coefficient according to $D^* = D_L/D_0$, where D_0 is the usual short time diffusion coefficient for DB, but it is the temperature and density dependent expresion in Eq. (30) for MD simulations. Thus, one can see that combining all the scaling rules in this work collapse all the data onto a single master curve.

Finally, in Fig. (2a) of Ref. [31] we showed, for a few systems, that the self-ISF follows the colloid-atomic long time equivalence. Fig. (2b) of the same reference, on the other hand, illustrated the equivalence at the level of the α-relaxation time. We provide further data for τ_α in our Fig. (19). In this figure the inset replots our previous

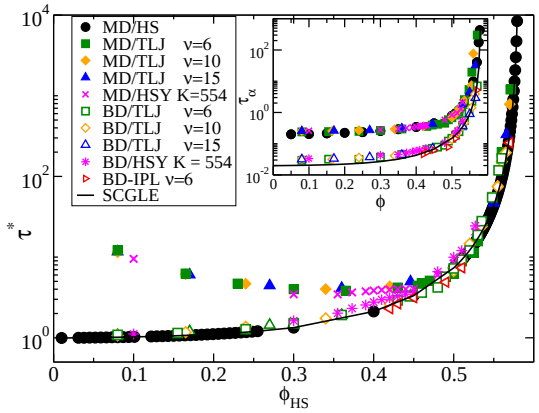

FIG. 19: Inset: α-relaxation time $\tau_\alpha(\phi)$ for Brownian and Newtonian liquids in HS units. Main panel: Data presented as $\tau^* \equiv k^2 D_0 \tau_\alpha$.

data for τ_α, in HS units, for both MD and BD dynamics. The main panel, on the other hand, plots (as in Ref. [31]) the dimensionless α-relaxation time $\tau^* \equiv k^2 D_0 \tau_\alpha$ in HS units, using the corresponding expression for D_0 for MD and DB simulations. This panel shows that all the systems are equivalent in the high volume fraction regime when plottend in the appropiate scale.

SUMMARY

In this work we have presented a simulation study on the structure and dynamics equivalence between fluids with model repulsive potentials and hard sphere fluids. We proposed a method to identify structurally equivalent systems that is better than other traditional approaches, especially for long ranged potentials.

ACKNOWLEDGMENTS: This work was supported by the Consejo Nacional de Ciencia y Tecnología (CONACYT, México), through grants No. 132540 and 182132.

[1] Angell C. A., Ngai K. L., McKenna G. B., McMillan P. F. and Martin S. F. 2000 J. Appl. Phys. **88** 3113
[2] M. D. Ediger, C. A. Angell, and S. R. Nagel, J. Phys. Chem. **100**, 13200 (1996)
[3] K. L. Ngai, D. Prevosto, S. Capaccioli and C. M. Roland, J. Phys.: Condens. Matter **20**, 244125 (2008)
[4] C. A. Angell, Science **267**, 1924 (1995).
[5] P. G. Debenedetti and F. H. Stillinger, Nature **410**, 359 (2001).
[6] F. Sciortino and P. Tartaglia, Adv. Phys. **54**, 471 (2005).
[7] *Jamming and Rheology: Constrained Dynamics on Microscopic and Macroscopic Scales*, edited by A. J. Liu and S. R. Nagel (Taylor & Francis, New York, 2001).
[8] N. Xu, T. K. Haxton, A. J. Liu, and S. R. Nagel, Phys. Rev. Lett. **103** 245701 (2009).
[9] L. Berthier and T. A. Witten, Europhys. Lett. **86**, 10001 (2009).
[10] H. Löwen, J. P. Hansen, and J. N. Roux, Phys. Rev. A **44**, 1169 (1991).
[11] G. Szamel and E. Flenner, Europhys. Lett., **67**, 779 (2004).
[12] A. M. Puertas, J. Phys.: Condens. Matter **22**: 104121 (2010).
[13] W. Götze, in *Liquids, Freezing and Glass Transition*, edited by J. P. Hansen, D. Levesque, and J. Zinn-Justin (North-Holland, Amsterdam, 1991).
[14] G. Szamel and H. Löwen, Phys. Rev. A **44**, 8215 (1991).
[15] J. L. Boon and S. Yip, *Molecular Hydrodynamics* (Dover Publications Inc. N. Y., 1980).
[16] M. Medina-Noyola, Faraday Discuss. Chem. Soc. **83**, 21 (1987).
[17] M. Medina-Noyola and J. L. del Río-Correa, *Physica 146A*, 483 (1987).
[18] L. Yeomans-Reyna and M. Medina-Noyola, Phys. Rev. E **62**, 3382 (2000).
[19] L. Yeomans-Reyna and M. Medina-Noyola, Phys. Rev. E **64**, 066114 (2001).
[20] L. Yeomans-Reyna, H. Acuña-Campa, F. Guevara-Rodríguez, and M. Medina-Noyola, Phys. Rev. E **67**, 021108 (2003).
[21] P.E. Ramírez-González *et al.*, Rev. Mex. Física **53**, 327 (2007).
[22] L. Yeomans-Reyna *et al.*, Phys. Rev. E **76**, 041504 (2007).
[23] R. Juárez-Maldonado *et al.*, Phys. Rev. E **76**, 062502 (2007).
[24] P. E. Ramírez-González and M. Medina-Noyola, Phys. Rev. E **82**, 061503 (2010); ibid. Phys. Rev. E **82**, 061504 (2010).
[25] P. E. Ramírez-González and M. Medina-Noyola, Phys. Rev. E **82**, 061503 (2010); ibid. Phys. Rev. E **82**, 061504 (2010).
[26] P. E. Ramírez-González and M. Medina-Noyola, J. Phys.: Cond. Matter, **21**, 75101 (2009).
[27] P. E. Ramírez-González, L. López-Flores, H. Acuña-Campa, and M. Medina-Noyola, Phys. Rev. Lett. **107**, 155701 (2011).
[28] H. C.Andersen, J. D. Weeks and D. Chandler, Phys. Rev. A **4**, 1597 (1971).
[29] J.P. Hansen and I.R. McDonald, *Theory of Simple Liquids* (Academic Press Inc., 1976)
[30] P. Mendoza-Méndez, L. López-Flores, A. Vizcarra-Rendón, L. E. Sánchez-Díaz, and M. Medina-Noyola, arXiv:1203.3893v1 [cond-mat.soft].
[31] L. López-Flores, L. L. Yeomans-Reyna, M. Chávez-Páez, and M. Medina-Noyola, J. Phys.: Condens. Matter, **24** 375107 (2012).
[32] G. Nägele, *Phys. Rep.* **272**, 215 (1996).
[33] K.J. Gaylor, I.K. Snook, W. van Megen, and R.O. Watts, J. Phys. A **13**, 2513 (1980).
[34] M.P. Allen and D.J. Tildesley, *Computer Simulation of Liquids*, (Oxford, University Press, 1887.)
[35] T.S. Grigera and G. Parisi, Phys. Rev. E **63**, 45102(R), (2001).

[36] D. Dubbeldam, D.C. Ford, D.E. Ellis, and R.Q. Snurr, Mol. Phys. **35**, 1084 (2009).
[37] J.S. van Duijneveldt and D. Frenkel, J. Chem. Phys. **96**, 4655 (1992).
[38] G. Pérez-Ángel et al., Phys. Rev. E **83**, 060501 (2011).
[39] J. K. Percus and G. J. Yevick, Phys. Rev. **110**, 1 (1957).
[40] M. S. Wertheim, Phys. Rev. Lett. **10**, 321 (1963).
[41] L. Verlet and J.-J. Weis, Phys. Rev. A **5** 939 (1972).
[42] F. de J. Guevara-Rodríguez and M. Medina-Noyola, Phys. Rev. E **68**, 011405 (2003).
[43] J. L. Lebowitz, Phys. Rev. **133**, A825 (1972).
[44] K. Hiroike, Mol. Phys. **33**, 1519 (1977); ibid, J. Phys. Soc. Jpn. **27**, 1415 (1969).
[45] P. N. Pusey in *Liquids, Freezing and Glass Transition*, edited by J. P. Hansen, D. Levesque, and J. Zinn-Justin (Elsevier, Amsterdam, 1991), Chap. 10.
[46] I. M. de Schepper, E. G. D. Cohen, P. N. Pusey, and H. N. W. Lekkerkerker, J. Phys. Condens. Matter. 1, 6503 (1989); P. N. Pusey, H. N. W. Lekkerkerker, E. G. D. Cohen, and I. M. de Schepper, Physica A 164, 12 (1990).
[47] H. Löwen, T. Palberg, and R. Simon, Phys. Rev. Lett. **70**, 1557 (1993)
[48] S. Chapman and T. G. Cowling, *The Mathematical Theory of Nonuniform Gases*, 2nd ed.; Cambridge University Press: Cambridge, U.K. (1952).
[49] D.A. McQuarrie, *Statistical Mechanics*, Harper and Row, N.Y. (1975).
[50] S. Chandrasekhar, Rev Mod. Phys. **15**: 1 (1943).
[51] B. Cichocki and K. Hinsen, Physica A **187**, 133 (1992).
[52] M. Tokuyama, H. Yamazaki, and Y. Terada, Phys. Rev. E 67, 062403 (2003).
[53] P.R. ten Wolde, M. J. Ruiz-Montero, and Daan Frenkel, Physical Rev. Letts. **75** 2714 (1995).
[54] M. Schmiedeberg, T.K. Haxton, and A.J. Liu, Europhys. Letts. **96**, 36010 (2011).
[55] E. Lange, J.B. Caballero, A.M. Puertas, and M. Fuchs, J. Chem. Phys. **130**, 174903 (2009).
[56] L. López-Flores, et. al., Europhys. Letts. **99**, 46001 (2012).